

PAPER • OPEN ACCESS

Near-infrared PbS quantum dots functionalized with affibodies and ZnPP for targeted imaging and therapeutic applications

To cite this article: Ali W Al-Ani *et al* 2021 *Nano Ex.* 2 040005

View the [article online](#) for updates and enhancements.

You may also like

- ['Green'-synthesized near-infrared PbS quantum dots with silica-PEG dual-layer coating: ultrastable and biocompatible optical probes for *in vivo* animal imaging](#)
D Wang, J Qian, F Cai et al.
- [Tuning the optoelectronic properties of PEDOT:PSS-PVP core-shell electrospun nanofibers by solvent-quantum dot doping and phase inversion](#)
M I Mendoza-Diaz, D F Garcia-Gutierrez, S Sepulveda-Guzman et al.
- [Nonlinear Properties Of Water-soluble Ag₂S And PbS Quantum Dots Under Picosecond Laser Pulses](#)
Qing Chang, Ying Gao, Xiwen Liu et al.



The Electrochemical Society
Advancing solid state & electrochemical science & technology

241st ECS Meeting

May 29 – June 2, 2022 Vancouver • BC • Canada

Abstract submission deadline: Dec 3, 2021

Connect. Engage. Champion. Empower. Accelerate.
We move science forward



Submit your abstract





PAPER

Near-infrared PbS quantum dots functionalized with affibodies and ZnPP for targeted imaging and therapeutic applications

OPEN ACCESS

RECEIVED

1 July 2021

REVISED

25 October 2021

ACCEPTED FOR PUBLICATION

27 October 2021

PUBLISHED

11 November 2021

Original content from this work may be used under the terms of the [Creative Commons Attribution 4.0 licence](#).

Any further distribution of this work must maintain attribution to the author(s) and the title of the work, journal citation and DOI.



Ali W Al-Ani¹ , Francesco Zamberlan^{1,2}, Lenny Ferreira¹, Tracey D Bradshaw³ , Neil R Thomas^{1,*} and Lyudmila Turyanska^{4,*}

¹ Biodiscovery Institute, School of Chemistry, University of Nottingham, Nottingham, NG7 2RD, United Kingdom

² School of Chemistry, University of Glasgow, Joseph Black Building, G12 8QQ, Glasgow, United Kingdom

³ Biodiscovery Institute, School of Pharmacy, University of Nottingham, University Park, Nottingham, NG7 2RD, United Kingdom

⁴ Centre for Additive Manufacturing, Faculty of Engineering, University of Nottingham, University Park, Nottingham, NG7 2RD, United Kingdom

* Authors to whom any correspondence should be addressed.

E-mail: Neil.Thomas@nottingham.ac.uk and Lyudmila.Turyanska@nottingham.ac.uk

Keywords: affibody, PbS QDs, zinc(II) protoporphyrin IX, HER2, breast cancer, quantum dots

Supplementary material for this article is available [online](#)

Abstract

We report a new theranostic device based on lead sulfide quantum dots (PbS QDs) with optical emission in the near infrared wavelength range decorated with affibodies (small 6.5 kDa protein-based antibody replacements) specific to the cancer biomarker human epidermal growth factor receptor 2 (HER2), and zinc(II) protoporphyrin IX (ZnPP) to combine imaging, targeting and therapy within one nanostructure. Colloidal PbS QDs were synthesized in aqueous solution with a nanocrystal diameter of ~5 nm and photoluminescence emission in the near infrared wavelength range. The Z_{HER2:432} affibody, mutated through the introduction of two cysteine residues at the C-terminus (Afb2C), was used as capping ligand to form Afb2C-PbS QDs that have a high binding affinity for HER2, which is overexpressed in several types of cancer including breast cancer. Afb2C-PbS QDs were further modified by conjugation with ZnPP, which acts as an anticancer agent. The biological activity of these QDs was tested against SKBR3 (HER2-positive) and MDA-MB-231 (HER2-normal) breast cancer cells, with results showing that ZnPP-Afb2C-functionalized PbS QDs were successfully targeted to the HER2-overexpressing cancer cells and induced cell apoptosis thanks to the conjugation with ZnPP. These results expand the use of the QD nanoplatfrom with the formulation of novel nanomaterials for targeted delivery and combined imaging and therapy via direct surface-protein interaction.

Introduction

The development of theranostic agents for simultaneous disease detection and targeted therapy has attracted considerable attention in recent years and brought significant advances to cancer treatments [1, 2]. This has been achieved by using drug delivery vehicles, such as polymer-based nanoparticles [3], protein nanocages [4], or liposomes, to encapsulate imaging and therapeutic agents, and also by direct attachment of ligands to the surface of solid colloidal nanoparticles (e.g. semiconductor quantum dots (QDs), silver, gold or iron oxide nanoparticles) [5–7]. In particular, the use of semiconductor QDs offers the benefit of tunable optical emission [8] with *in vivo* imaging potential in the near-infrared (NIR) wavelength range where absorption of biological tissues is low. This is offered by QDs based on IV–VI group elements (PbS, PbSe) [9–13]. One of the areas where NIR-emitting nanomaterials are currently being investigated for detection and treatment is the targeting of breast cancers [14, 15], exploiting the elevated expression of estrogen receptor alpha (ER α) and/or epidermal growth factor receptor 2 (HER2). Currently, focus has shifted towards HER2-based detection and therapy as this receptor is amplified or overexpressed in up to ~30% of breast cancers and other malignancies notably gastric

cancers, while not expressed in immunohistochemically detectable quantities in normal adult tissue cells. HER2 overexpression is associated with poor prognosis in the absence of systemic therapy [16].

To date, molecules that have been explored for breast cancer-specific targeting include naturally recognized protein capsules, such as ferritin, and immunoglobulin G (IgG) antibodies [17–19]. A promising alternative are affibodies (Afb), which can replace antibodies as the targeting functionality of biopharmaceuticals for diagnostic and therapeutic applications [20, 21]. The $Z_{\text{HER2:432}}$ Afb is a non-immunoglobulin-based, highly specific binding protein of small size (58 amino acids, ~6.5 kDa), engineered from a 3-helix bundle Z derived from staphylococcal protein A, with a high binding affinity for HER2 ($K_D \sim 22$ pM) [22, 23]. It is known for fast and reversible folding, high solubility in aqueous solutions, an attachment surface as large as an antibody antigen binding pocket and for being easily expressed in high yields in *E. coli*, thus making it an ideal targeting agent for cancer therapies [24–26], which is slowly making its way in theranostic applications [27]. The immobilization of Afb's was recently demonstrated on nanoparticles, including Ag_2S and InAs/InP/ZnSe core/shell/shell QDs through the use of a heterobifunctional linker conjugation on PEG-capped QD surfaces, or *via* electrostatic interactions [28–30], but no direct surface attachment has been reported to date.

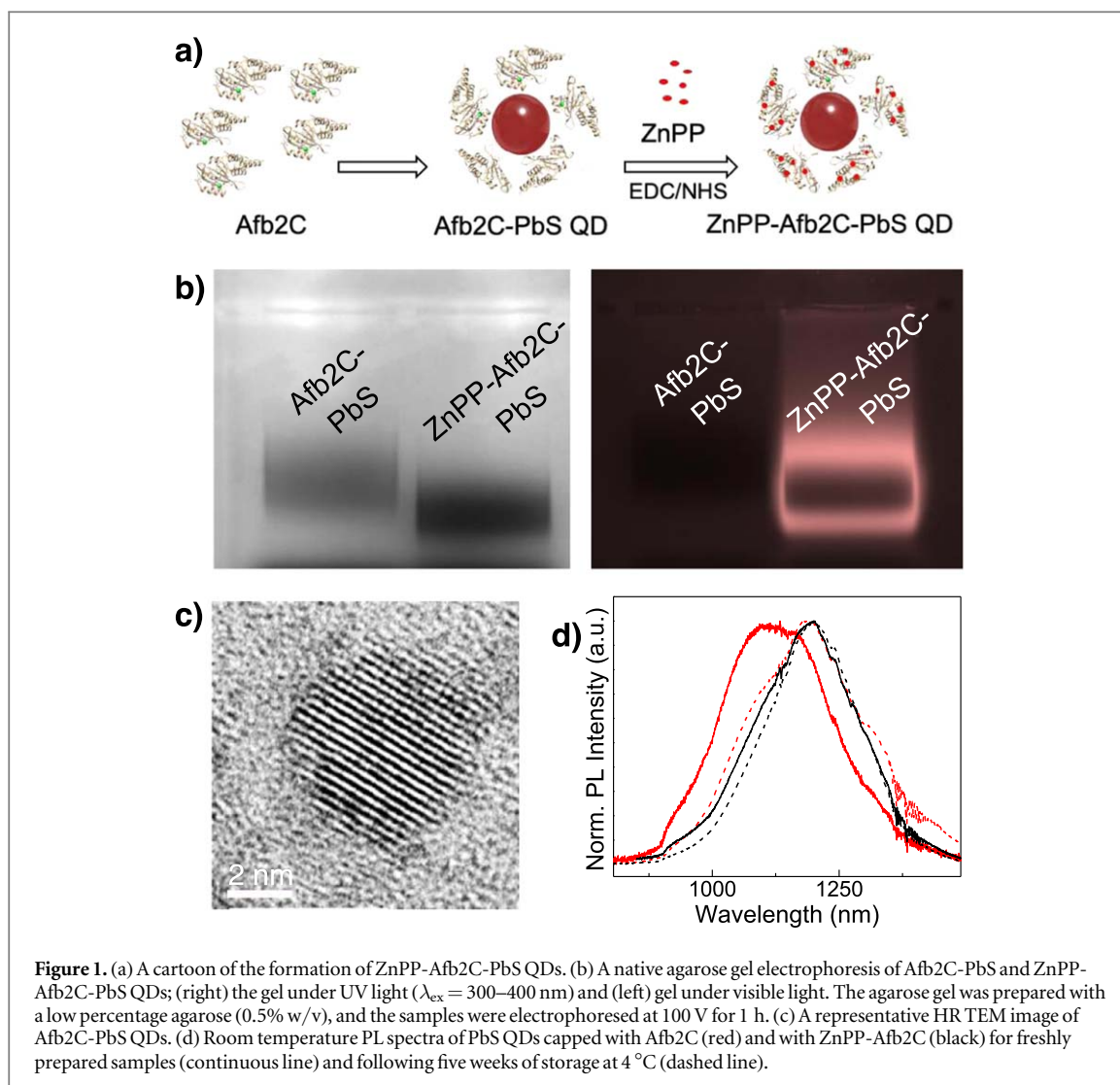
Current breast cancer therapy comprises several partially successful drugs; however, new therapeutic strategies are needed, especially for metastatic and drug-resistant breast cancers [31, 32]. Recently, the therapeutic anticancer activity of zinc(II) protoporphyrin IX (ZnPP) was demonstrated with the inhibition of hemoxygenase-1 [33, 34], an enzyme which is highly overexpressed in cancerous tissues and exerts a cytoprotective effect by neutralizing oxidative stress in cells [35]. At the same time, ZnPP can also induce cell apoptosis by generating singlet oxygen species upon irradiation with blue light ($\lambda_{\text{ex}} = 425$ nm), allowing for applications in cancer photodynamic therapy [36–39]. Despite the number of promising advances, including nano-engineering of drug delivery systems [40] as well as surface decoration of QDs [41] combined targeting, anticancer activity and imaging within one nano-construct is yet to be achieved. Facile procedures for the controllable and direct attachment of targeting and therapeutic agents onto the QDs surface still remain challenging.

In this work we describe a one-pot synthesis of water-soluble and biocompatible near-infrared-emitting PbS QDs functionalized with Afb and ZnPP for diagnosis and therapy (figure 1(a)). The simultaneous attachment of both $Z_{\text{HER2:432}}$ Afb and ZnPP molecules onto a QD surface will produce a novel theranostic agent that combines the benefits of selective targeting and specific cellular uptake induced by Afb, the NIR fluorescent bioimaging of QDs and the anticancer activity of ZnPP. The $Z_{\text{HER2:432}}$ Afb was genetically modified to introduce two specific mutations to incorporate two cysteine residues at its C-terminus—G82C and S83C. The Afb2C generated with two thiol groups allows for a bidentate interaction of the protein with the QD and consequently stronger binding to the QD surface, hence increasing the long-term stability of the QD-protein conjugate [39]. Afb2C-PbS QDs were further modified by conjugating ZnPP at the lysine residues of Afb2C to produce ZnPP-Afb2C-PbS QDs, which were found to be stable in solution and optically active in the NIR. The effect of these QDs on HER2-overexpressing (HER2+) SKBR3 cells was explored to confirm selectivity and activity and is reported herein. The approach reported here for the synthesis of novel nanocomposites that combine in one structure targeting, imaging and therapy is relevant for the advancement of theranostics into the clinic.

Results and discussion

Site-directed mutagenesis was performed to create a specific change on the $Z_{\text{HER2:342}}$ affibody (Afb) DNA sequence. In the pJexpress401 plasmid, the Afb2C gene was designed with an N-terminal His-tag, and two mutations (G82C and S83C) which were introduced at its C-terminus; we note that these residues were not critical for the Afb binding to HER2 (Supplementary Information, SI1). The mutant Afb2C protein was successfully expressed in BL21 (DE3) *E. coli* and purified using nickel(II)-immobilized metal affinity chromatography (IMAC) followed by further purification by size exclusion chromatography (SEC). The presence and purity of the Afb2C protein were confirmed by SDS-PAGE. To examine the stability of the Afb2C structure under the conditions used for QD synthesis, the secondary structure of the Afb2C protein was determined at pH 7.0 and pH 11.0 using circular dichroism (CD) spectroscopy (see Supplementary Information, Figure S2), indicating that the α -helical secondary structure of the Afb2C found at pH 7.0 was retained at pH 11.0.

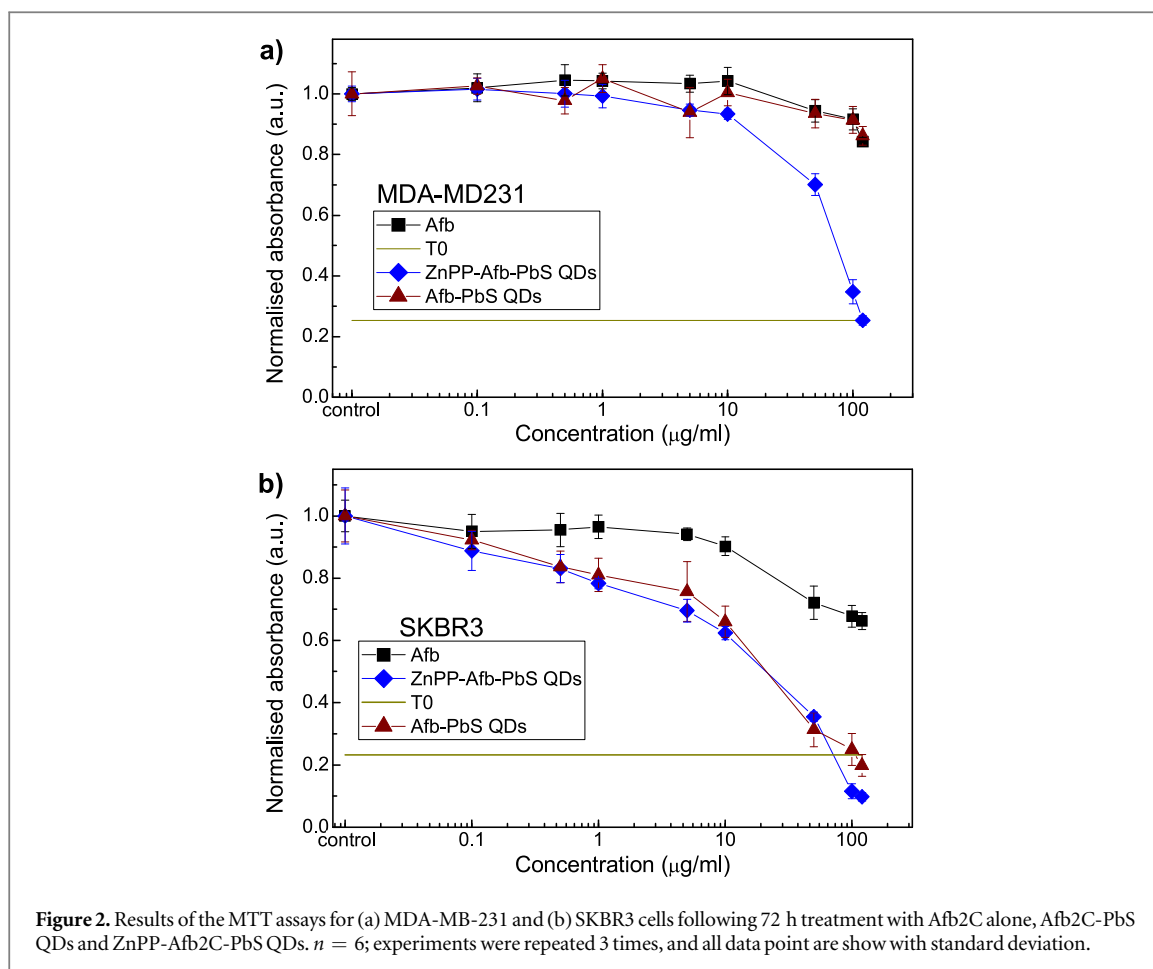
The Afb2C was used as the capping ligand in a one-pot synthesis of PbS QDs. The QDs were synthesized in aqueous solution following modified procedure reported in [11, 13] with molar ratio of Pb:S = 1:0.3 (figure 1(a)). In this process, the presence of two cysteine sites in Afb2C offers bidentate interaction with the QD surface and greater stability, as was previously demonstrated for other bidentate ligands such as dihydrolipoic acid [42]. Then, ZnPP was conjugated *in situ* to Afb2C-PbS QDs by reacting the lysine residues located within the Afb2C protein with the NHS-activated carboxyl groups on the protoporphyrin, forming a stable amide bond—



we did not investigate further which lysines had been involved in the process. Figure 1(b) shows the native agarose gel electrophoresis spots of Afb2C-PbS QDs and the ZnPP-Afb2C-PbS QDs. Under illumination with UV light ($\lambda = 300\text{--}400\text{ nm}$), no fluorescent bands were observed on native PAGE gels of Afb2C-PbS QDs as these emit in the NIR region, while clear red fluorescence was observed for ZnPP-Afb2C-PbS QDs, as expected from the presence of ZnPP, confirming successful conjugation (figure 1(b)). We also explain the lower migration spot for ZnPP-Afb2C-PbS QDs with their faster migration compared to Afb2C-PbS QDs, due the change in net charge (pI) derived from the neutralization of lysine residues after conjugation, despite their overall larger size.

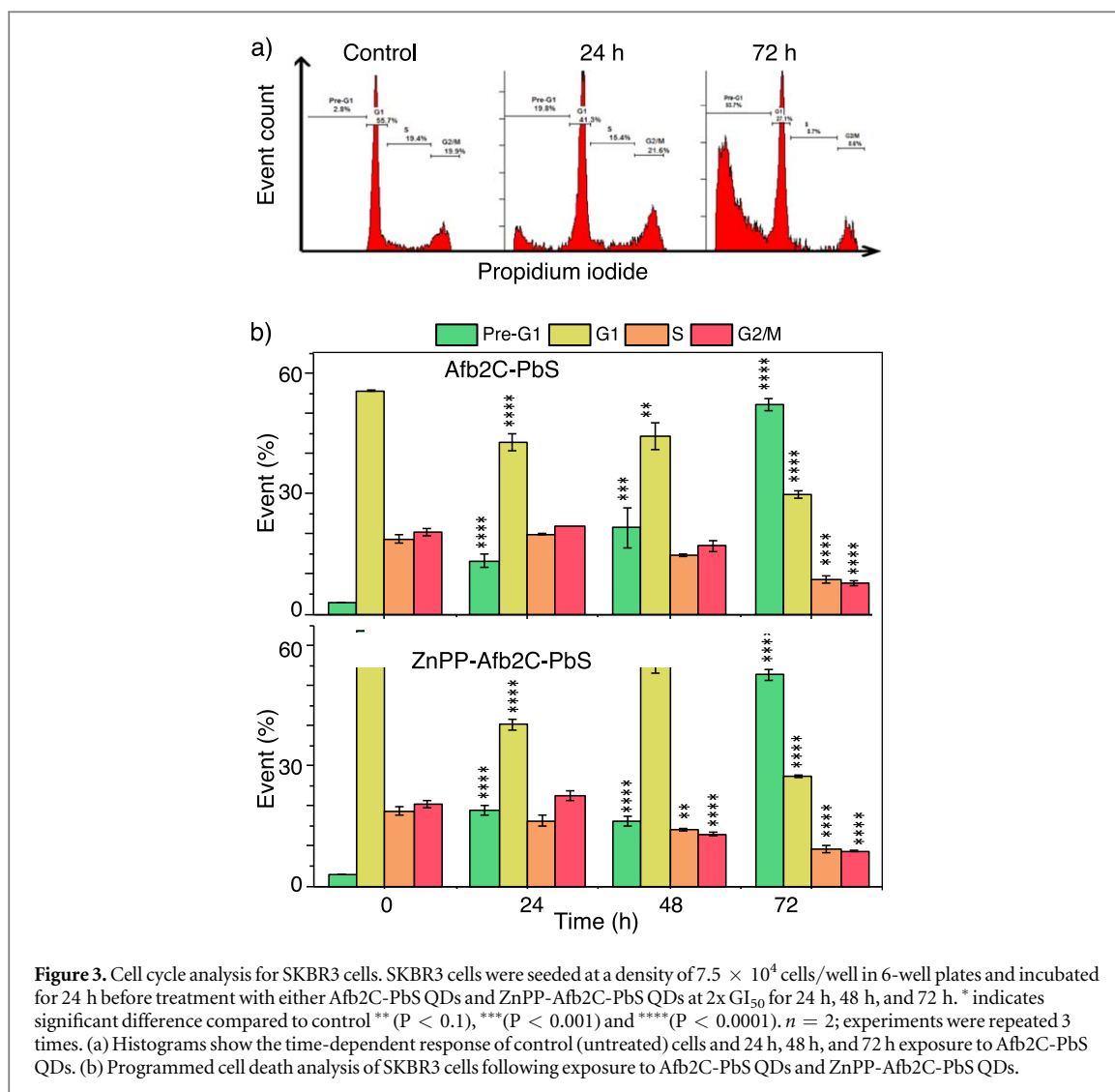
The synthesized QDs have room temperature photoluminescence (PL) centered at $\lambda_{\text{PL}} \sim 1180\text{ nm}$ (figure 1(d)), similar to that expected from this synthesis method with thioglycerol/dithioglycerol capping ligands, and suggest that the Afb2C can be used instead of dithioglycerol to provide efficient passivation of the QD surface. Significantly, attachment of ZnPP does not affect the optical properties of the QDs [11, 43]. We note that the presence of both Afb2C and ZnPP on the QD surface provides more efficient surface passivation and greater stability against Ostwald ripening, compared to Afb2C only passivated QDs. Both QD solutions have comparable PL peak position for the fully ripened samples (figure 1(d)). The TEM images revealed that the PbS QDs had a spherical shape, high crystallinity and an average diameter of $5 \pm 1\text{ nm}$ (figure 1(c) and Supplementary Information, figures S3, S4), with the observed size comparable to that estimated from the PL peak position using model developed by Moreels *et al* [44]. Both Afb2C-PbS QDs and ZnPP-Afb2C-PbS have long term colloidal stability with respect to morphological and optical properties over a period of at least three months (stored under nitrogen at $T = 4\text{ }^{\circ}\text{C}$).

The 3-(4,5-dimethylthiazol-2-yl)-2,5-diphenyltetrazolium bromide (MTT) assay was used to study the growth inhibitory effects of Afb2C-PbS QDs and ZnPP-Afb2C-PbS QDs in SKBR3 and MDA-MB-231 cell lines. SKBR3 is a human breast cancer cell line expressing between 1,000,000 and 2,000,000 HER2 per cell, whereas non-cancerous cells display $\sim 20,000$ HER2 per cell [45, 46]. Consequently, the SKBR3 cell line is used as a positive control in HER2 assays and is considered a suitable preclinical model for screening therapies that target



HER2 [45, 46]. Clinically, HER2+ breast cancers develop resistance to trastuzumab (Herceptin[®]), a therapeutic antibody developed to target and treat this type of breast [32]. MDA-MB-231 triple negative breast cancer (TNBC) cells, instead, display ~ 100 -fold lower HER2. Also lacking estrogen and progesterone receptors, TNBCs are associated with poor prognosis, exhibiting highly invasive characteristics [47, 48]. Following 72 h exposure, dose-dependent growth inhibition was observed in SKBR3 cells in the presence of Afb2C-PbS QDs, with a mean GI_{50} value of $26 \mu\text{g ml}^{-1}$ (Afb2C concentration 4.5 mg ml^{-1} during synthesis), which is significantly lower than that observed for Afb2C alone and ZnPP alone ($GI_{50} > 100 \mu\text{g ml}^{-1}$, figure 2 and Supplementary Information, figure S5) [37]; no growth inhibitory effects were observed in MDA-MB-231 cells $< 100 \mu\text{g ml}^{-1}$ (figure 2 and Supplementary Information, figure S5). These results suggest that the Afb2C is recognized by HER2 receptors as predicted and leads to selective and enhanced uptake of the nanoplateform in the HER2 + SKBR3 cells. In this case the activity is due to the presence of PbS QDs, which have been shown previously to be non-toxic to normal cells (MRC-5) but to induce cytotoxic effects in cancerous cells [11]. Comparable results are observed following exposure to ZnPP-Afb2C-PbS QDs (figure 2 and Supplementary Information, figure S6). The lower GI_{50} value in SKBR3 cells confirms Afb-induced targeting. We note that the greater growth inhibition observed in MDA-MB-231 exposed to ZnPP-Afb2C-PbS, compared to Afb2C-PbS only, is likely due to extracellular activity of ZnPP conjugated on our nanoplateform, as this is able to generate ROS and inhibit hemoxygenase-1 and acts as photosensitizer [34, 37, 38]. It was shown previously that the anticancer activity of ZnPP is different in different cell lines and can be enhanced, e.g. by pre-treatment of cancer cells with agents affecting protein transportation [39].

To investigate further the nature of growth inhibitory activity, we performed cell cycle studies in SKBR3 cells. SKBR3 cells were exposed to Afb2C-PbS QDs or ZnPP-Afb2C-PbS QDs at a concentration of $2 \times GI_{50}$ value for 24 h, 48 h, and 72 h. The flow cytometry results (figures 3(a) and S7) revealed increasing populations in the pre-G1 phase with increasing exposure time. For Afb2C-PbS QDs the pre-G1 population increased from 13.3% after 24 h to 52.3% ($P < 0.0001$) after 72 h of treatment, and was accompanied by decreased G1, S and G2/M events (figure 3(b)). Similar changes were observed for ZnPP-Afb2C-PbS QDs, where the cell population in pre-G1 phase increased from 18.9% to 52.8% after 72 h treatment (figure 3(b)). The presence of significant pre-G1 events is indicative of DNA degradation and consequent cell apoptosis, previously reported following cancer cell exposure to PbS QDs [11]. Resistance to apoptosis is a hallmark of human cancer [49], thwarting



successful treatment; therefore, inducing apoptosis in cancer cells is a major goal of anticancer therapies. We expected that ZnPP-Afb2C-PbS QDs would exhibit augmented anti-proliferative effects due to conjugation with ZnPP, however, Afb2C-PbS QDs and ZnPP-Afb2C-PbS QDs had similar effects on the SKBR3 cell cycle. Our results suggest that conjugation of ZnPP with Afb2C-PbS QDs decreases the affinity of Afb for HER2 receptors and consequently reduces the effects of ZnPP-Afb2C-PbS QDs on HER2 + SKBR3 cells. The reduced dose of ZnPP-Afb2C-PbS QDs in these cells is therefore responsible for their similar growth inhibitory effect to Afb2C-PbS QDs.

Further flow cytometric studies were performed to investigate the mechanism of cell death, using dual propidium iodide (PI) and annexin V staining of cells. The results confirmed cell death by apoptosis (early- and late-stage) for Afb2C-PbS QDs and late-stage apoptosis-detection for ZnPP-Afb2C-PbS QDs following exposure to $2 \times GI_{50}$ for 24 h, 48 h and 72 h, where apoptotic populations gradually increased with time to >20% (Supplementary Information, SI2). Afb2C-PbS QDs induced late apoptosis in SKBR3 cells after 24 h of treatment and their effect increased by 44% after 72 h. In addition, SKBR3 cell necrosis was also detected after 72 h of treatment: we conclude that Afb2C-PbS QDs induced SKBR3 cell apoptosis and necrosis, the major cell death pathways. For ZnPP-Afb2C-PbS QDs, cells underwent necrosis after 24 h of exposure, doubling to 23.1% after 72 h of treatment (supplementary information SI2, figure S11 (available online at stacks.iop.org/NANOX/2/040005/mmedia)). This indicates that the nanocomposites have a potent anti-proliferative effect on SKBR3 cells and that they force most cells to undergo necrosis bypassing programmed cell death: we conclude that conjugation of ZnPP with Afb2C-PbS QDs switches SKBR3 cell fate from apoptosis to necrosis, suggesting a sudden catastrophic cytotoxic effect for this nanocomposite compared to Afb2C-PbS QDs.

The ability of ZnPP-Afb2C-PbS QDs to enter and localize in cells was monitored using flow cytometry in SKBR3 and MDA-MB-231. Cells were incubated with ZnPP-Afb2C-PbS QDs at $2 \times GI_{50}$ for 3 h. The uptake of

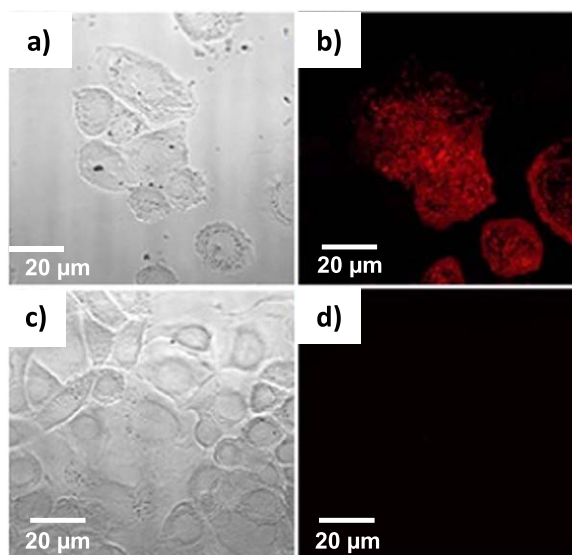


Figure 4. Confocal images. (a) The brightfield view and (b) the fluorescence emitted from SKBR3 cells after exposure to ZnPP-Afb2C-PbS QDs for 3 h. (c) The brightfield and (d) the fluorescence images of untreated SKBR3 cells. Cells were seeded at a density of 10×10^3 cells/well in 8-well plate and treated with ZnPP-Afb2C-PbS QDs at $2 \times GI_{50}$. For both experiments, ZnPP was excited at 425 nm and the emitted light was detected at 594 nm.

ZnPP-Afb2C-PbS QDs was ~ 2 -times higher in HER-2 + SKBR3 cells compared to MDA-MB-231 cells (Supplementary Information, S13).

Confocal microscopy imaging was used to detect intracellular fluorescence of ZnPP-Afb2C-PbS QDs ($\lambda_{em} = 593$ nm, excitation with 425 nm, figure 4 and supplementary information, S13) and indicated that the agent is distributed in the cell cytoplasm; the non-uniform fluorescence with small brighter areas suggests uptake by endocytosis. Despite reporting significant agent uptake, no detectable fluorescence was measured in MDA-MB-231 cells by confocal microscopy (supplementary information, figure S13): we explain this fact with the presence of ZnPP that leads to cell death, as reported previously [37], a consequence of high metabolic turnover and genetic instability, making cells more susceptible to ROS generation and its consequences. Confocal images also revealed changes in morphology of both studied cell lines following treatment with ZnPP-Afb2C-PbS QDs, such as blebbing of the cell membrane, which is associated with late-stage apoptosis and necrosis; that this has occurred is strongly indicated by intracellular PI accumulation observed in flow cytometric assays, and corroborates an apoptotic mechanism of cell death.

In our recent work, we demonstrated deep tissue imaging with near-infrared PbS QDs [13]. The results in the present report on novel PbS QDs directly coated with the anti-HER2 Afb2C protein and conjugated with ZnPP indicate realistic prospects for their utilization in cancer imaging and therapy. The enhanced uptake demonstrated for Afb2C-functionalized nanoparticles is of benefit for drug delivery and imaging of HER2-overexpressing cancer cells [50]. With the present report, we have also demonstrated the possibility of using the QDs' surface for the direct incorporation of other active principles within the same nanostructure for theranostic applications, which could be expanded to other agents, e.g. the therapeutic antibodies pertuzumab and trastuzumab [50].

In conclusion, we have produced stable near-infrared colloidal PbS QDs directly passivated with a small protein Afb2C and further functionalized with ZnPP. The Afb2C provides targeting to the HER2 + cells while ZnPP contributed therapeutic activity against breast cancer cells. The novel theranostic ZnPP-Afb2C-PbS QDs demonstrated selective anticancer activity, targeting HER2 + cells and triggering apoptotic cell death; the bioimaging application has also been reported *in vitro*, and further studies are required to assess the activity of these QDs *in vivo* and to explore their theranostic potential.

Materials and methods

DNA mutagenesis

DNA sequence gene encoding Afb in pJexpress401 plasmid was mutated by replacing glycine and serine at positions 82 and 84 respectively with cysteine using Q5[®] Site-Directed Mutagenesis according to the manufacturer's instructions (New England Biolabs) to produce Afb2C. Afb2C in pJexpress401 plasmid was

amplified by transforming in the DH5 α calcium competent cells and then the plasmid was extracted and purified using the Wizard Plus[®] SV Miniprep kit (Promega).

Afb2C expression and purification

For the Afb2C expression, isopropyl β -D-1-thiogalactopyranoside (IPTG) (1 mM, Fisher Scientific) was added for 4 h at $T = 37^\circ\text{C}$ into *E. coli* BL21 (DE3) culture containing the pJexpress401:Afb2C plasmid. The Luria Bertani (LB) medium supplemented with kanamycin ($50\ \mu\text{g ml}^{-1}$, Apollo Scientific) was used. Cells were collected by centrifugation (2500 g, 25 min, $T = 4^\circ\text{C}$), resuspended in binding buffer (40 ml of 20 mM Tris pH 8.3 (Fisher Scientific), 10 mM imidazole (Sigma Aldrich)), 1 mM phenyl methyl sulfoxide (PMSF) (Sigma Aldrich) and sonication. The sample was then centrifugation (35000 g, 25 min, $T = 4^\circ\text{C}$) and the supernatant was loaded on a 5 ml nickel column (GE Healthcare). 5 ml of binding buffer (20 mM of Tris pH 8.6, 10 mM of imidazole) was used for washing; washing was repeated 3-times. Afb2C was then eluted using a linear gradient of increasing imidazole concentration up to 500 mM. The purified Afb2C was loaded into 6–8 K MWCO dialysis tubing (Spectrum Laboratories) and dialyzed against two changes of Tris buffer (2 l, 20 mM Tris pH 8.3, 1 mM DTT) for ~ 16 h. Tricine-SDS-gel electrophoresis was used to confirm presence of Afb2C. All fractions containing Afb2C were loaded on a size exclusion column (Superdex 75 10/300 GL) and were analyzed using Tricine-SDS-PAGE. NANO Drop A-1000 spectrophotometer was used to measure the absorbance of the samples (extinction coefficient = $8,480\ \text{M cm}^{-1}$), which were used to calculate the concentration of Afb2C. The yield of purified protein was 4 mg per L of culture.

MALDI-TOF MS

Bruker Matrix Assisted Laser Desorption/Ionization (MALDI-TOF, Bruker Ultraflex III) MS was used to analyze the samples following the LP-44 kDa method. Samples were prepared by mixing $5\ \mu\text{l}$ of protein with $10\ \mu\text{l}$ of the saturated sinapic acid solution (molar ratio of sinapic acid to acetonitrile is 1:2, with added 0.1% (v/v) of trifluoroacetic acid). Samples were loaded onto the plate and dried at room temperature. The spectrum was analyzed using flexControl (Ultraflex) 3.0 software. *Circular dichroism (CD) spectroscopy*. The Afb2C ($0.5\ \mu\text{g ml}^{-1}$) was analyzed in 20 mM Tris buffer at pH 7.0 and pH 11.0 using a CD spectrometer (Chirascan Plus Spectroscopy). Samples were dialyzed with the desired buffer at 4°C overnight and the pH was adjusted using 10 mM H_2SO_4 .

Synthesis of Afb2C-PbS QDs

Afb2C in 70% (v/v) $(\text{NH}_4)_2\text{SO}_4$ was pelleted and washed with Tris buffer (20 mM Tris pH 8.3) including 70% (v/v) $(\text{NH}_4)_2\text{SO}_4$ and pelleted again to remove the DTT. The pellet was dissolved in 1.7 ml of 0.0167 M aqueous solution of lead acetate trihydrate ($\text{Pb}(\text{CH}_3\text{CO}_2)_2 \cdot 3\text{H}_2\text{O}$) (Sigma), and 1.7 ml of Tris buffer (40 mM Tris pH 8.3) was added. The pH was adjusted to 11.0 using 0.1 M NaOH. The reaction mixture was stirred for 30 min under N_2 . Then 0.25 ml of 0.1 M Na_2S was added to the reaction mixture. The color of the solution changed to dark brown indicating the formation of PbS QDs. The Afb2C-PbS QDs solution was stirred for 30 min. Finally, the product was dialyzed against Tris buffer (20 mM Tris pH 11.0) overnight to remove excess reactants. The QD solutions were stored under a nitrogen atmosphere at 4°C in the dark.

Labelling of Afb2C-PbS QDs with ZnPP

Afb2C-PbS QDs were dialyzed against PB (20 mM NaH_2PO_4 pH 11.0) overnight at 4°C . ZnPP labelling was performed modified Thermo Scientific protocol. To produce the activated protoporphyrin-*N*-hydroxysuccinimide ester (ZnPP-NHS), $100\ \mu\text{l}$ of ZnPP in DMSO (30 mM) were mixed with $12\ \mu\text{l}$ of 500 mM of 1-(3-dimethylaminopropyl)-3-ethylcarbodiimide hydrochloride (EDC) in MES buffer (0.1 M MES (2-[*N*-morpholino]ethanesulfonic acid) pH 6). The reaction mixture was agitated at room temperature for 1 min. Following incubation, $12\ \mu\text{l}$ of *N*-hydroxysuccinimide (NHS) (500 mM) in MES buffer was added. The reaction mixture was agitated for further 15 min at room temperature before the solution was centrifuged at room temperature (4000 g, 15 min) and any precipitates were discarded. Afb2C-PbS QDs were mixed with a 10-fold excess of the activated ZnPP-NHS ester under ambient conditions. The reaction mixture was protected from light and was gently agitated overnight at room temperature. The product was centrifuged at 5000 g for 10 min to remove unreacted protoporphyrin and then dialyzed against PB (20 mM NaH_2PO_4 pH 8.3) overnight at 4°C . The QD solutions were stored under a nitrogen atmosphere at 4°C in the dark.

Optical and morphological characterization

The PL of PbS QDs was analyzed using a Horiba Jobin Yuon Ltd HR800 LabRam setup equipped in InGaAs detector. The excitation was provided with a He-Ne laser ($\lambda = 633\ \text{nm}$, $P = 10^4\ \text{W cm}^{-2}$). For transmission electron microscopy (TEM) studies, PbS QDs at a concentration of $0.1\ \text{mg ml}^{-1}$ were deposited on a graphene-

oxide-coated Cu grid (Agar Scientific) and TEM images were recorded on the JEOL2100EX microscope operating at 120 keV.

In vitro studies

SKBR3 and MDA-MB-231 breast cancer cell lines were cultured under optimum conditions in RPMI nutrient medium (Sigma-Aldrich) supplemented with 10% fetal bovine serum (FBS; Sigma Aldrich), and sub-cultivated twice weekly to maintain logarithmic growth. For MTT assays, cells were seeded into 96-well plates at a density of approximately 3×10^3 cells/well in 180 μ l medium and allowed to adhere to the plates by incubating at 37 °C for 24 h. Serial dilution of Afb2C-PbS QDs or ZnPP-Afb2C-PbS QDs were prepared and 20 μ l per well was added to achieve a final concentration of Afb2C from 0.1 μ g ml⁻¹ to 120 μ g ml⁻¹. After 72 h exposure, MTT solution (50 μ l 2 mg ml⁻¹) was added to each well and incubated for 3 h. The medium was aspirated and DMSO (150 μ l) was added to dissolve the formazan crystals. The absorbance was measured at 550 nm using an En Vision 2104 Multilabel microplate reader (PerkinElmer).

For cell cycle and Annexin V assays, cells were seeded in a 6-well plate at a density of 7.5×10^4 cells/well in 2 ml of RPMI nutrient medium supplemented with 10% FBS, and allowed 24 h to adhere. The cells were treated with 2x GI₅₀ concentrations of Afb2C-PbS QDs and ZnPP-Afb2C-PbS QDs for 24 h, 48 h and 72 h. The medium, containing dead cells, was collected into labelled fluorescence activated cell sorter (FACS) tubes and kept on ice. The remaining adherent cells were trypsinized with 500 μ l of 1 × trypsin-EDTA before pooling with the medium containing dead cells. The cells were centrifuged at 4 °C (1200 rpm) for 5 min, the supernatant was removed, and the cell pellets washed with 1 ml of PBS followed by another cycle of centrifugation. The supernatant was decanted.

For cell cycle assays, cell pellets were resuspended in 500 μ l of cold hypotonic fluorochrome solution (50 μ g ml⁻¹ PI (Sigma-Aldrich), 0.1 mg ml⁻¹ ribonuclease A (Sigma-Aldrich), 0.1% v/v Triton X-100 (Sigma-Aldrich), 0.1% w/v sodium citrate (Sigma-Aldrich) dissolved in PBS), protected from light and stored overnight at 4 °C. Samples were vortexed and analyzed on a Beckman Coulter Epics-XL MCL flow cytometer. At least 10 000 events were recorded for each sample. The results were analyzed using EXPO32 software.

For annexin V assays, the Annexin V-FITC/PI (AV/PI) (BD Pharmingen) kit was used. To FACS tubes containing cell pellets, 400 μ l of 1 × annexin binding buffer and 10 μ l of PI solution were added, samples were vortexed and incubated for 10 min at room temperature without light. Samples were analyzed within 1 h on a Beckman Coulter Epics-XL MCL flow cytometer and at least 10 000 events were recorded for each sample. The results were analyzed using EXPO32 software.

The cellular uptake of ZnPP-Afb2C-PbS QDs was studied using flow cytometry. Cells were seeded at a density of 7.5×10^4 cells/well in 6 well plates in 2 ml of RPMI nutrient medium and allowed 24 h to adhere. The cells were treated with 2 × GI₅₀ concentration of ZnPP-Afb2C-PbS QDs for 3 h. The cells were then washed (2-times 2 ml of PBS), trypsinized (0.5 ml 0.25% w/v trypsin-EDTA), pooled (1 ml RPMI nutrient medium) and centrifuged for 5 min at 1200 g (Beckman Coulter Allegro). The cell pellet was further washed (2 × 1 ml PBS), centrifuged and resuspended in 0.5 ml of PBS. Astrios EQ flow cytometer (Beckman Coulter) with excitation at $\lambda_{ex} = 425$ nm and Kaluza Flow Cytometry software were adopted for analysis.

Confocal microscopy

Cells were seeded in an 8-well μ -slide confocal chamber (Ibidi GmbH, Munich, Germany) at a density of 7.5×10^4 per well. After overnight incubation, cells were treated with before treatment with 2 × GI₅₀ of ZnPP-Afb2C-PbS QDs. After 24 h exposure, cells were washed (3 × 0.2 ml PBS), fixed (0.2 ml 4% (v/v) formaldehyde, 20 min), then washed again (3 × 0.2 ml PBS). Fixed cells were stained with DRAQ5™ DNA stain, then washed (3 × 0.2 ml PBS). Confocal microscopy images were captured on LEICA DMI 4000 B using excitation wavelengths $\lambda_{ex} = 425$ nm and $\lambda_{em} = 593$ nm. ImageJ (Fiji) software was used for image analysis.

Statistical analysis

For all experiments, $n \geq 3$ internal replicates and $n \geq 3$ independent trials were conducted. Data were analyzed using one-way, two-way analyses of variance (ANOVAs), and t-tests; $p < 0.05$ identified significance.

Acknowledgments

The work was supported by the NC3Rs/EP SRC [grant number NC/L001861/1], the EP SRC Impact Acceleration Account [grant number EP/K503800/1], and the Ministry of Higher Education and Scientific Research in Iraq. The authors would like to acknowledge Dr Lei Zhang and Dr Mohammed Alnajjar for their lab assistance, Dr Michael W. Fay for TEM imaging. Authors acknowledge access to the facilities at the Nanoscale and Microscale Research Centre of University of Nottingham.

Data availability statement

The data that support the findings of this study are available upon reasonable request from the authors.

Author contributions

AWA performed the experimental studies with support from FZ and LF. TDB, NRT and LT conceptualized the research and provided project supervision. All co-authors contributed to data analysis, writing of the manuscript and approved submission.

Conflicts of interest

The authors declare no conflicting interests.

ORCID iDs

Ali W Al-Ani  <https://orcid.org/0000-0003-1597-0344>

Tracey D Bradshaw  <https://orcid.org/0000-001-8451-5092>

Neil R Thomas  <https://orcid.org/0000-0002-9260-5423>

Lyudmila Turyanska  <https://orcid.org/0000-0002-9552-6501>

References

- [1] Xie J, Lee S and Chen X 2010 *Adv. Drug Deliv. Rev.* **62** 1064–79
- [2] Yu M K, Park J and Jon S 2012 *Theranostics* **2** 3–44
- [3] Indoria S, Singh V and Hsieh M-F 2020 *Int. J. Pharm.* **582** 119314
- [4] Lee S, Pham T C, Bae C, Choi Y, Kim Y K and Yoon J (ed) *Coord. Chem. Rev.* 2020 **412** 213258
- [5] Hu X-L, Kwon N, Yan K-C, Sedgwick A C, Chen G-R, He X-P, James T D and Yoon J 2020 *Adv. Funct. Mater.* **30** 1907906
- [6] Barabadi H, Mahjoub M A, Tajani B, Ahmadi A, Junejo Y and Saravanan M 2019 *J. Clust. Sci.* **30** 259–79
- [7] Fan M, Han Y, Gao S, Yan H, Cao L, Li Z, Liang X-J and Zhang J 2020 *Theranostics* **10** 4944–57
- [8] Michalet X 2005 *Science* **307** 538–44
- [9] Hennequin B, Turyanska L, Ben T, Beltran A M, Molina S I, Li M, Mann S, Patane A and Thomas N R 2008 *Adv. Mater.* **20** 3592–6
- [10] Smith A M, Mancini M C and Nie S 2009 *Nat. Nanotechnol.* **4** 710–1
- [11] Bradshaw T D, Junor M, Patanè A, Clarke P, Thomas N R, Li M, Mann S and Turyanska L 2013 *J. Mater. Chem. B* **1** 6254–60
- [12] Sasaki A, Tsukasaki Y, Komatsuzaki A, Sakata T, Yasuda H and Jin T 2015 *Nanoscale* **7** 5115–9
- [13] Zamberlan F et al 2018 *J. Mater. Chem. B* **6** 550–5
- [14] Jin G, He R, Liu Q, Dong Y, Lin M, Li W and Xu F 2018 *ACS Appl. Mater. Interfaces* **10** 10634–46
- [15] Liu R, Hu C, Yang Y, Zhang J and Gao H 2019 *Acta Pharm. Sin.* **9** 410–20
- [16] Arteaga C L, Sliwkowski M X, Osborne C K, Perez E A, Puglisi F and Gianni L 2012 *Nat. Rev. Clin. Oncol.* **9** 16–32
- [17] Geninatti Crich S, Cadenazzi M, Lanzardo S, Conti L, Ruiu R, Alberti D, Cavallo F, Cutrin J C and Aime S 2015 *Nanoscale* **7** 6527–33
- [18] Bae Y H and Park K 2011 *J. Controlled Release* **153** 198–205
- [19] Garaud S, Zayakin P, Buisseret L, Rulle U, Silina K, de Wind A, Van den Eyden G, Larsimont D, Willard-Gallo K and Liné A 2018 *Front. Immunol.* **9** 2660
- [20] Löfblom J, Feldwisch J, Tolmachev V, Carlsson J, Ståhl S and Frejd F Y 2010 *FEBS Lett.* **584** 2670–80
- [21] Frejd F Y and Kim K-T 2017 *Exp. Mol. Med.* **49** e306
- [22] Trousil S, Hoppmann S, Nguyen Q-D, Kaliszczak M, Tomasi G, Iveson P, Hiscock D and Aboagye E O 2014 *Clin. Cancer Res.* **20** 1632–43
- [23] Ravalli A, da Rocha C G, Yamanaka H and Marrazza G 2015 *Bioelectrochemistry* **106** 268–75
- [24] Feldwisch J, Tolmachev V, Lendel C, Herne N, Sjöberg A, Larsson B, Rosik D, Lindqvist E, Fant G and Höidéén-Guthenberg I 2010 *J. Mol. Biol.* **398** 232–47
- [25] Sörensen J, Sandberg D, Sandström M, Wennborg A, Feldwisch J, Tolmachev V, Åström G, Lubberink M, Garske-Román U and Carlsson J 2014 *J. Nucl. Med.* **55** 730–5
- [26] Liu H, Seijsing J, Frejd F Y, Tolmachev V and Gräslund T 2015 *Int. J. Oncol.* **47** 601–9
- [27] Nabil G, Bhise K, Sau S, Atef M, El-Banna H A and Iyer A K 2019 *Drug Discov. Today* **24** 462–91
- [28] Gao J, Chen K, Miao Z, Ren G, Chen X, Gambhir S S and Cheng Z 2011 *Biomaterials* **32** 2141–8
- [29] Pérez-Treviño P, la Cerda H H-D, Pérez-Treviño J, Fajardo-Ramírez O R, García N and Altamirano J 2018 *Transl. Oncol.* **11** 672–85
- [30] Zhang Y, Zhao N, Qin Y, Wu F, Xu Z, Lan T, Cheng Z, Zhao P and Liu H 2018 *Nanoscale* **10** 16581–90
- [31] Loibl S and Gianni L 2017 *Lancet* **389** 2415–29
- [32] Kunte S, Abraham J and Montero A J 2020 *Cancer* **126** 4278–88
- [33] Hirai K, Sasahira T, Ohmori H, Fujii K and Kuniyasu H 2007 *Int. J. Cancer* **120** 500–5
- [34] Kongpetch S, Kukongviriyapan V, Prawan A, Senggunprai L, Kukongviriyapan U and Buranrat B 2012 *PLoS One* **7** e34994
- [35] Kang K A et al 2012 *Tumor Biol.* **33** 1031–8
- [36] Regehly M, Greish K, Rancan F, Maeda H, Böhm F and Röder B 2007 *Bioconjug. Chem.* **18** 494–9
- [37] Al-Ani A W, Zhang L, Ferreira L, Turyanska L, Bradshaw T D and Thomas N R 2019 *Nanomedicine Nanotechnol. Biol. Med.* **20** 102005
- [38] Fang J, Liao L, Yin H, Nakamura H, Subr V, Ulbrich K and Maeda H 2015 *Future Sci. OA* **1** 3
- [39] Wang S, Hannafon B N, Lind S E and Ding W-Q 2015 *PLoS One* **10** e0127413

- [40] Nabil G, Bhise K, Sau S, Atef M, El-Banna H A and Iyer A K 2019 *Drug Discovery Today* **24** 462–92
- [41] Sharmiladevi P, Girigoswami K, Haribabu V and Girigoswami A 2021 *Mater. Adv.* **2** 2876–91
- [42] Medintz I L, Uyeda H T, Goldman E R and Mattoussi H 2005 *Nat. Mater.* **4** 435–46
- [43] Turyanska L, Bradshaw T D, Li M, Bardelang P, Drewe W C, Fay M W, Mann S, Patanè A and Thomas N R 2012 *J. Mater. Chem.* **22** 660–5
- [44] Moreels I et al 2009 *ACS Nano* **3** 3023–30
- [45] Trempe G L 1976 *Breast Cancer: A Multidisciplinary Approach* ed G St-Arneault et al (Berlin: Springer) p. 33–41
- [46] Wong D J L and Hurvitz S A 2014 *Ann. Transl. Med.* **2** 122
- [47] Prat A, Parker J S, Karginova O, Fan C, Livasy C, Herschkowitz J I, He X and Perou C M 2010 *Breast Cancer Res.* **12** R68
- [48] Cailleau R, Young R, Olivé M and Reeves W J Jr 1974 *JNCIJ. Natl. Cancer Inst.* **53** 661–74
- [49] Hanahan D and Weinberg R A 2011 *Cell* **144** 646–74
- [50] Orlova A, Magnusson M, Eriksson T L J, Nilsson M, Larsson B, Höidén-Guthenberg I, Widström C, Carlsson J, Tolmachev V and Ståhl S 2006 *Cancer Res.* **66** 4339–48